Acta Cryst. (1998). A**54**, 374–387

Geometrical Model of the Phase Transformation of Decagonal Al–Co–Ni to its Periodic Approximant

MATTHIAS HONAL, TORSTEN HAIBACH AND WALTER STEURER*

Laboratory of Crystallography, Swiss Federal Institute of Technology Zurich, CH-8092 Zurich, Switzerland. E-mail: steurer@kristall.erdw.ethz.ch

(Received 1 September 1997; accepted 8 December 1997)

Abstract

Based on computer simulations in direct as well as in reciprocal space, a geometrical model for the transformation from decagonal Al–Co–Ni to an orientationally twinned crystalline nanodomain structure is derived. Mapping the atomic positions of the quasicrystal onto the corresponding positions of its (4, 6)-approximant leads to a patchwork-like arrangement of crystalline nanodomains. The atomic displacements necessary to transform the quasicrystal into the nanodomain structure are determined locally. The optimum orientation of the approximant unit cells building the nanodomains is obtained by minimizing the sum of the corresponding displacements. Approximately 50% of the resulting atomic shifts are less than 1 Å, and more than 90% less than 1.5 Å. These results are verified by comparison with previous experimental observations. An intermediate state of the transformation is related to a one-dimensional quasicrystal. It is interpreted within the approach of a linear growth model. Slight changes of the approximant lattice parameters as induced by temperature strongly influence domain size and distribution. Correlations between the nanodomains are referred to the discrete periodic average structure common to both the decagonal phase and the approximant structure.

1. Introduction

Crystalline phases showing a close structural relationship to quasicrystals are well known for icosahedral as well as for decagonal structures. In the embedding approach (*cf.* Yamamoto, 1996, and references therein), d-dimensional (dD) quasiperiodic structures result from an irrational cut of an n-dimensional (nD with $n > d$) hypercrystal structure with dD physical space. If the cut becomes rational by shearing the nD hypercrystal parallel to perpendicular space, a periodic crystal structure called rational approximant is obtained. Both, approximant and quasicrystal, show locally the same structure motifs due to their hyperspace relationship (*cf.* Goldman & Kelton, 1993, and references therein). Consequently, the intensity distribution of diffraction patterns of quasicrystals and their approximants are very similar. Moreover, in the case of multiply twinned microcrystalline approximants, the diffraction patterns cannot be distinguished from those of quasicrystals by standard low-resolution X-ray experiments (Estermann *et al.*, 1994).

First experimental investigations on the phase transformations for Al–Cu–Co-type decagonal quasicrystals (with a characteristic average translation period of about 4 Å) have been performed using HRTEM and selected-area electron diffraction (SAED) (Hiraga *et al.*, 1991; Audier *et al.*, 1993). Transitions induced under an electron or Ar^+-ion beam have been reported (Zhang & Urban, 1992; Qin *et al.*, 1995). More recently, temperature-dependent neutron powder diffraction experiments and X-ray single-crystal studies have been performed (Dong *et al.*, 1991; Fettweis *et al.*, 1995; Baumgarte *et al.*, 1997). All these experiments are evidence of a reversible decagonal quasicrystal-to-crystal transformation leading to a domain structure on the nanometre scale of orientationally twinned approximants. Experimental studies from high-resolution electron microscopy (HRTEM) lead to a domain size of a few hundred ångströms (Hiraga *et al.*, 1991; Song *et al.*, 1993), while from high-resolution X-ray diffraction coherence lengths of several thousand ångströms have been reported (Kalning *et al.*, 1997).

The main emphasis is put on the atomic structure and lattice parameters of the crystalline phase forming these domains. CsCl-type structures, structures with b.c.c. or f.c.c. lattices, have been reported with lattice parameters of about 3 Å (Zhang & Urban, 1992; Qin *et al.*, 1995) as well as different orthorhombic phases (*cf.* Dong *et al.*, 1991) and monoclinic (or centred orthorhombic) structures. These approximants show the periodicity of the quasicrystal (4 Å) in the unique c direction and $a = b \simeq 20$, $\simeq 32$ or $\simeq 52$ Å, $\gamma = 144$ or 108°, respectively (*cf.* Hiraga *et al.*, 1991; Audier *et al.*, 1993; Fettweis *et al.*, 1995). Additionally, the transition passes through an intermediate one-dimensional quasicrystalline phase (Kalning *et al.*, 1997). However, a uniform interpretation of all the different observations has not been given yet and none of the approximant structures involved in

the transition mechanism has been determined up to now.

Most theoretical studies on quasicrystal–crystal transformations use the nD approach describing the transformation in terms of continuous hyperlattice deformations by phason strain (a shear deformation of the hyperlattice). Alternatively, a description in terms of tilings and reshuffling of atoms by phason flips is applied (*cf.* Yacamán & Torres, 1993). Janssen (1991) discussed direct-space deformations of the six-dimensional hyperlattice to describe formally a phase transformation from an icosahedral phase to a rational approximant. The action of linear phason strain transforming the decagonal quasicrystal to its monoclinic approximants *via* a one-dimensional quasicrystal can also be described in reciprocal space (Zhang & Kuo, 1990; Zhang *et al.*, 1993). The shift of Bragg peaks is a function of the perpendicular-space component of the diffraction vector $\mathbf{H}^{\perp}$. It is described by the product $M\mathbf{H}^{\perp}$, with the shear matrix M.

An alternative method is the description in terms of the deviation from a reference lattice. Duneau & Oguey (1990) proved that, for every quasiperiodic structure fulfilling particular conditions, a mapping to a periodic reference lattice with bounded displacements exists. Tolédano & Dmitriev (1996) demonstrated that points where mass densities of quasicrystal and approximant coincide form a periodic lattice (T lattice). Hence, the structure is identical at the lattice nodes and similar in the vicinity of the nodes, whereas in regions between two nodes any similarity is lost. The T lattice is incommensurate to the corresponding approximant. Based on the T lattice, a quasicrystal–crystal phase transformation could be described partly by a local homogeneous deformation. For the regions without similarity, splitting and fusion of atomic sites are postulated, together with diffusion of atoms and a residual amount of disorder. Multiple twinning and/or microcrystalline states are proposed leading to small rotational (and translational) ordered domains of large structural elements of the quasicrystal.

The monoatomic transformation model proposed by Coddens & Launois (1991) is based on a direct comparison of quasicrystalline and approximant structure on a rather small scale (~80 Å). Structural changes are related to a phason flip mechanism. Only one distance (between the minima of a double-well potential) is used to correlate all atoms in the quasicrystal with atomic positions in the approximant structure. This is always possible because all positions are described by the same $\mathbb{Z}$-module. Consequently, the smaller the distances between quasicrystal and approximant atomic positions are, the more consecutive phason flips are necessary for each atom. As flip sequences might even involve positions that are occupied, a whole cascade of correlated jumps would be necessary to achieve a transformation of a larger area. However, a real-space mechanism for the quasicrystal–crystal transformation on the atomic scale in agreement with experimental observations has not been derived yet.

2. Characteristics of the structure models

2.1. *Quasicrystal*

An idealized four-dimensional structure model of one quasiperiodic atomic layer has been constructed based on the structure of decagonal $Al_{70}Co_{15}Ni_{15}$, space group $P10_5/mmc$, $a_q^* = 0.2636\,(1)$ Å^{-1}, $a_5^* = 0.24506\,(3)$ Å^{-1}; $d_q = 3.3931\,(9)$ Å, $d_5 = 4.0807\,(3)$ Å and corresponding $a_q = 3.794\,(1)$ Å, $a_5 = 4.0807\,(3)$ Å (Steurer *et al.*, 1993). Two atomic surfaces with regular pentagonal shape (radius $\lambda = 2/5a_q^*$) are at special positions $\frac{2222}{5555}$ and $\frac{4444}{5555}$ on the body diagonal of the hyperrhombohedral four-dimensional unit cell. The first one consists of Al centred by a τ-times $[\tau = 2\cos(\pi/5) \simeq 1.618\ldots]$ smaller inner decagon of transition metal (TM), the latter consists of Al only. As Co and Ni differ by only one electron, they are not distinguishable in conventional X-ray experiments and all simulations were performed with TM set to Co.

The structure of the quasicrystal layer is a subset of a Penrose tiling with skinny and fat rhombi of $2\tau a_q/5 \simeq 2.456$ Å edge length. Since only one of the vertices on the shorter diagonal of the skinny rhomb is occupied, the shortest distance in the plane is exactly the length of the rhomb edge. The three-dimensional physical space structure is built up by two of these quasiperiodic layers with stacking sequence Aa (a denotes layer A rotated by $\pi/5$) at relative z positions $\frac{1}{4}$ and $\frac{3}{4}$ according to the five-dimensional space group $P10_5/mmc$.

2.2. *Rational approximant*

Lattice parameters for the rational (n, m) approximant can be derived using the quasicrystal constant a_q according to Edagawa *et al.* (1991):

$$\begin{aligned} a_o &= a_q \tfrac{2}{5}\tau^{n+2}(3-\tau)^{1/2}(2+\tau)^{1/2} \\ b_o &= a_q \tfrac{2}{5}\tau^{m+2}(3-\tau)^{1/2} \\ a_q &= 3.794\,\text{Å}. \end{aligned} \tag{1}$$

Here, the (4, 6)-approximant is constructed with the lattice parameters $a_o \simeq 60.89$, $b_o \simeq 83.81$ Å in the orthorhombic C-centred setting, *i.e.* $a_m = b_m \simeq 51.80$ Å, $\gamma = 108°$ in the monoclinic one. The periodicity in the c direction is ~4.08 Å for both the quasicrystal and the approximant, the stacking sequence is the same. This specific approximant was found in the systems Al–Cu–Co(–Si) and Al–Co–Ni by HRTEM, SAED and high-resolution X-ray diffraction (Song *et al.*, 1993; Fettweis *et al.*, 1994; Kalning *et al.*, 1994). The structure is built from the pentagonal clusters (diameter ~20 Å) that decorate the quasiperiodic tiling (Fig. 1). As a result of

lowering the symmetry from $P10_5/mmc$ to $Ccmm$, the approximant structure is generated in five possible orientations, each one rotated relative to each other by $2\pi i/5$ ($i = 1, \ldots, 4$).

2.3. *Point densities*

The point density of the quasiperiodic layer can be derived from that of the Penrose tiling (Steurer & Haibach, 1998*a*) [equation (2)]. Considering only two atomic surfaces present, each τ-times larger than in the original Penrose tiling, results in equation (3).

$$\rho_{\text{pen}} = \tfrac{5}{2} a_q^{*2} (2+\tau)^{1/2}/\tau^3 \qquad (2)$$

$$\begin{aligned} \rho_q &= \rho_{\text{pen}}[\tau^4/(1+\tau^2)] \\ &= \tfrac{5}{2} a_q^{*2} \tau/(2+\tau)^{1/2} \\ &\simeq 0.147768593\ldots. \end{aligned} \qquad (3)$$

With the number of atoms N_{Al} in one layer of the monoclinic approximant unit cell, the point density of the approximant layer is

$$\begin{aligned} \rho_m &= \tfrac{5}{2} a_q^{*2} (2+\tau)^{1/2} N_{\text{Al}}/\tau^{14} \\ &\simeq 0.147768385\ldots \quad \text{with} \quad N_{\text{Al}} = 377. \end{aligned} \qquad (4)$$

Thus, the difference in point densities of $\sim$0.2 in 10^6 is physically irrelevant.

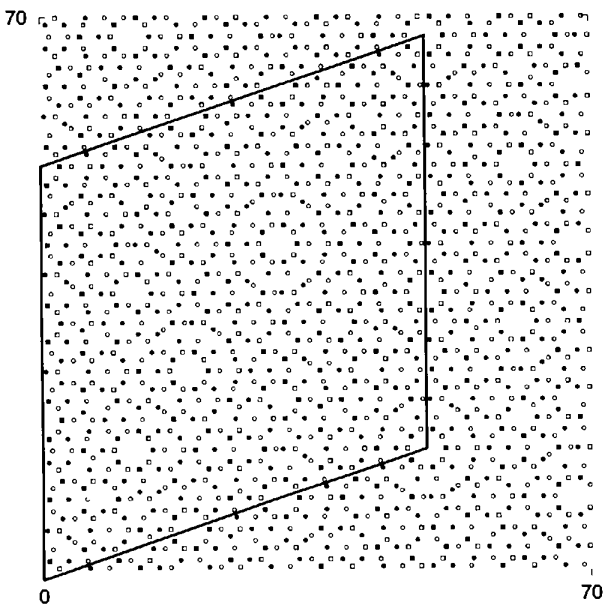

Fig. 1. 70 × 70 Å section of the idealized quasicrystal structure projected along $\mathbf{a}_5$. One monoclinic (4, 6)-approximant unit cell is marked. Al positions are given by circles, TM atoms by squares; filled symbols denote an atomic layer at $a_5/4$, open symbols at $3a_5/4$.

3. Simulation technique

All calculations have been performed with the model structures described above, generated up to a size of 8000 × 8000 × 4 Å, including about 18 million atoms.

3.1. *Atomic displacements*

The atomic displacements necessary for a displacive phase transformation are determined by mapping the quasicrystal structure onto the approximant structure. For each atomic position in the quasiperiodic layer, all possible displacement vectors to the nearest positions in the approximant layer are calculated within a radius of the shortest interatomic distance (2.456 Å). The shortest vectors are kept as minimum atomic displacement for subsequent calculations. Rejected atoms, as well as atoms without one-to-one correspondence within the given radius, are collected separately. This procedure is iterated until no more new atomic displacements are obtained. The displacement maps (*cf.* Fig. 2) are calculated for each orientation of the approximants.

3.2. *Domain formation*

To preserve the basic structural elements ($\sim$20 Å clusters), the domain formation is restricted to complete monoclinic approximant unit cells. The information on the displacements is encoded in coordinates of the corresponding approximant unit cell, together with its origin and orientation and the integral atomic shifts per unit cell (Fig. 3). A nanodomain structure (Figs. 5 and 6) is achieved by selecting locally the approximant orientation with the minimum integral shifts. One approximant lattice is taken as a reference coordinate system. Around each lattice node, within a circle of diameter equal to the long diagonal of the unit cell, the approximant orientation with smallest integral shifts is selected. This keeps the overlap small at the cost of partly unfilled domain boundaries. The algorithm produces a kind of texture, *i.e.* slight deviations from the fivefold symmetrical domain distribution expected. It does not influence, however, the general appearance of the nanodomain structure.

The determination of distances, integral shifts per unit cell and the selection of domain orientations are all performed in the first layer as the second layer is constrained by symmetry relations. Models centred at the unique 10_5 axis of the quasicrystal exhibit a fivefold symmetrical domain distribution in any case (biased by some texture effects). Consequently, to avoid such unique settings, all calculations were performed in the positive quadrant only, to enlarge the area concerned without effecting the computational effort.

3.3. *Simulating X-ray diffraction*

For X-ray diffraction simulations, all models are expanded in the periodic direction to a full period according to their symmetry. Explicit Fourier transformation is calculated for one approximant unit cell in each of the five possible orientations, followed by a summation of the complex structure factors over all unit-cell origins. All calculations are performed with a resolution up to 2.5×10^{-5} Å^{-1}. No fast Fourier transform (FFT) algorithm or factorization is used to avoid inherent restrictions that could veil intensity information between Bragg reflections. For the largest model (8000 × 8000 × 4 Å), a nanodomain structure of ±8000 Å along x and y directions was generated by applying fivefold symmetry to the data of the positive quadrant.

Fourier transformation of the first quadrant and its rotated counterparts with a subsequent summation of intensities gives a diffraction pattern of incoherently scattering regions. This can be expected in the case of a multi-nucleation regime with independent domains.

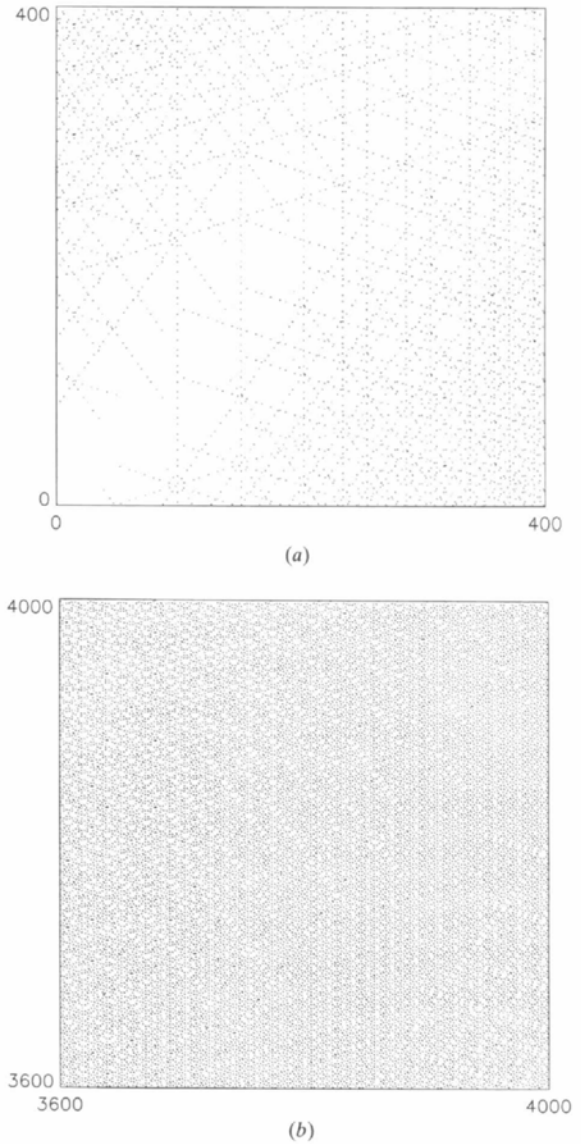

Fig. 2. Displacements for a transformation of decagonal Al–Co–Ni into a single-crystalline (4, 6)-approximant. The origins of the quasicrystal and the approximant coincide at (0, 0). (*a*) Displacements next to the origin, (*b*) 3600 Å away (both 400 × 400 Å sections). It is obvious that in (*b*) many more displacements are necessary for the quasicrystal–crystal transformation.

4. Direct-space properties of the nanodomain structure

4.1. *Displacement statistics*

Mapping the quasicrystal to a single approximant yields 93% of all resulting displacements smaller than the shortest interatomic distance (2.456 Å). 7% of the displacement exceed the maximum radius and can be assigned to atoms without one-to-one correspondence in quasicrystal and approximant. They are partly related to triangles of Al positions (with two edges at 2.456 Å and the third one τ-times larger) found in different orientations within the alternating Al/TM decagons of the cluster. Mapping these triangles according to the shortest possible displacements may allow two pairs of atoms to be connected by small vectors, while the vector for the third pair exceeds the allowed value. If all atoms are considered simultaneously, all pair vectors would be small enough to be accepted. Although two vectors are getting longer, the sum of the three shifts would be even smaller. However, an algorithm not only

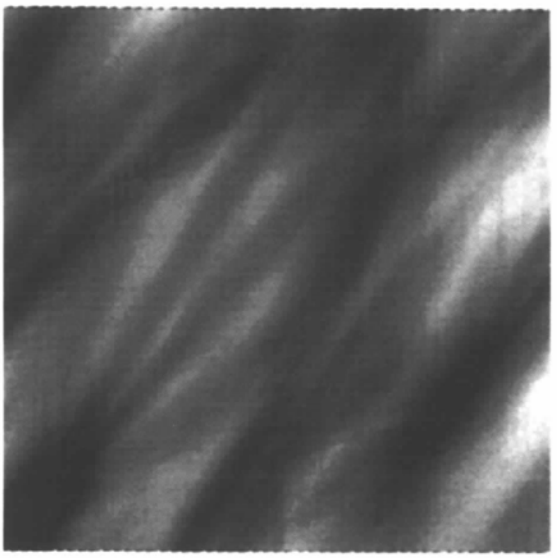

Fig. 3. Total sum of atomic shifts per approximant unit cell displayed as grey values, ranging from black (minimum sum of shifts) to white (maximum) for an 8000 × 8000 Å single-crystalline approximant.

taking pair correlations into account but minimizing also the global sum of displacements could not be applied owing to the huge number of atoms. Additional atoms without one-to-one mapping occur if quasicrystal atoms fall into the empty pentagons (edge length τ times 2.456 Å) of atomic positions in an approximant cluster and *vice versa*.

Within the first 800 × 800 Å, null vectors, resulting from absolute coincidence of atomic positions in quasicrystal and approximant, and simple flips [vector length $2a_q/(5\tau) \simeq 0.938$ Å] dominate (Figs. 2 and 3). 95.7% of all shifts are of these lengths, with a ratio of nearly one to one, while 4.0% of the vectors are of 1.80 Å length. By enlarging the model, many other displacements with varying length occur. 49.0% of the shifts mapping the 8000 × 8000 Å quasicrystal to a single-crystalline approximant are less than 1 Å while 8.3% are larger than 1.5 Å. However, the formation of a nanodomain structure instead of a single approximant reduces the total sum of shifts by one fifth (Fig. 4).

As the atomic species were not distinguished, chemical disorder is induced. To obtain a chemically

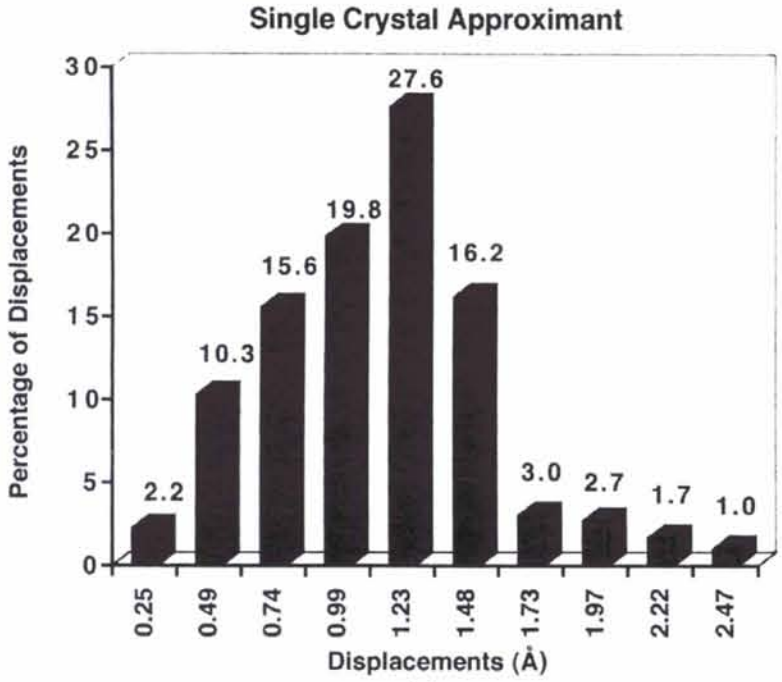

(*a*)

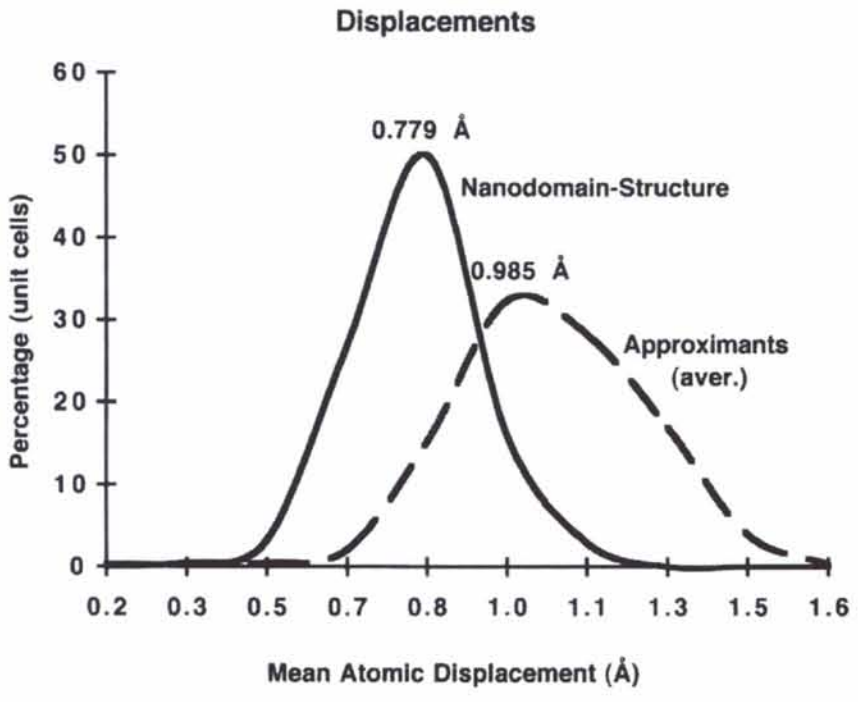

(*b*)

Fig. 4. (*a*) Bar graph displaying all displacements obtained from mapping an 8000 × 8000 Å quasicrystal to a single-crystalline approximant. Numbers given on the *x* axis are maximum values [Å] for the counting interval above. (*b*) Distribution functions of the atomic displacements necessary for the transformation to a single-crystalline approximant (broken line) and an orientationally twinned nanodomain structure (solid line) as calculated from the simulations.

Fig. 5. Nanodomain structure calculated in an area of $0 \leq x, y \leq$ 8000 Å. The different domain orientations are indicated by different colours.

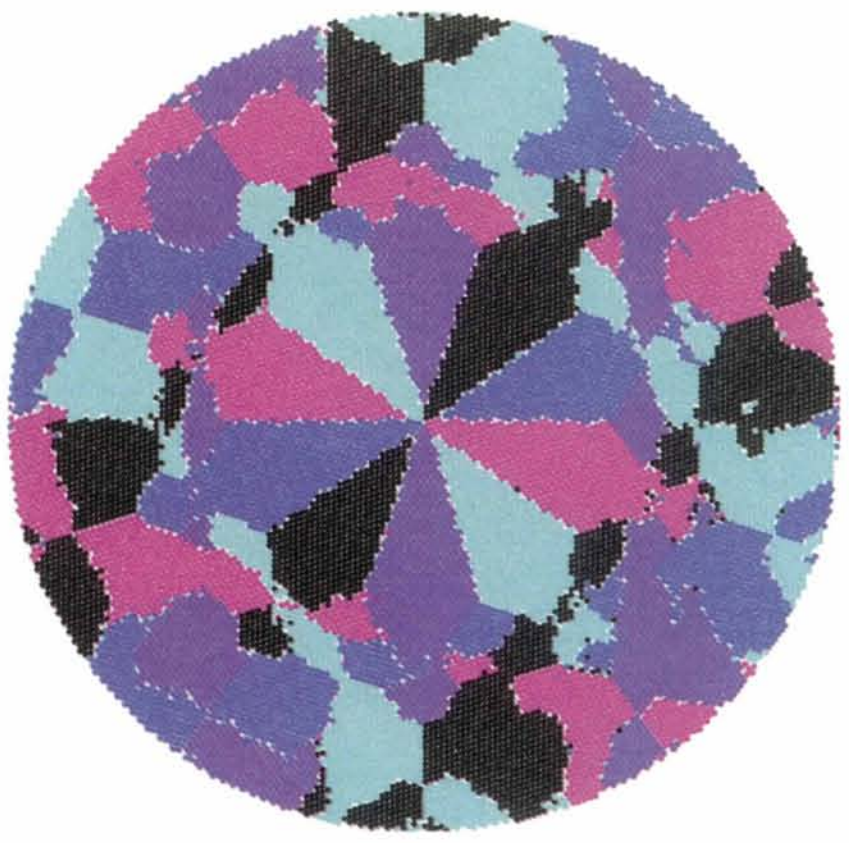

Fig. 6. Nanodomain structure calculated in an area of 8000 Å in diameter around the origin of the quasicrystal model. The different domain orientations are indicated by different colours.

ordered 8000 × 8000 Å approximant, single-crystal atomic diffusion for 39.9% of the atoms would be necessary. Up to now, no single crystals of the (4, 6)-Al–Co–Ni approximant could be prepared. Hence, atomic diffusion may indeed be kinetically hindered. The formation of a nanodomain structure as simulated, however, keeps the chemical disorder smaller. A certain amount of disorder seems to be likely as indicated by diffuse scattering on X-ray diffraction patterns. For a small model, restricting displacement vectors to chemically identical atoms only enlarges the total amount of displacements necessary as well as the number of rejected atoms with respect to the constant shift limit. The resulting nanodomain structure differs slightly from the one observed concerning the domain distribution.

4.2. *Domain distribution and boundaries*

The 8000 × 8000 Å nanodomain structure (Fig. 5) is built from unit cells of the approximants. It contains 22151 unit cells that mimic the symmetry of the quasicrystal. Considering a model of equal size centred at the origin (*i.e.* ±4000 × ±4000 Å), nearly 3450 cells for all possible approximant orientations are distributed in an almost tenfold manner (Fig. 6). In the inner part, dendritic growth along the long diagonal of the monoclinic unit cell dominates, while in the outer parts relatively large irregular-shaped domains are found. As most domains exceed 1000 Å in diameter, only a few small domains are present.

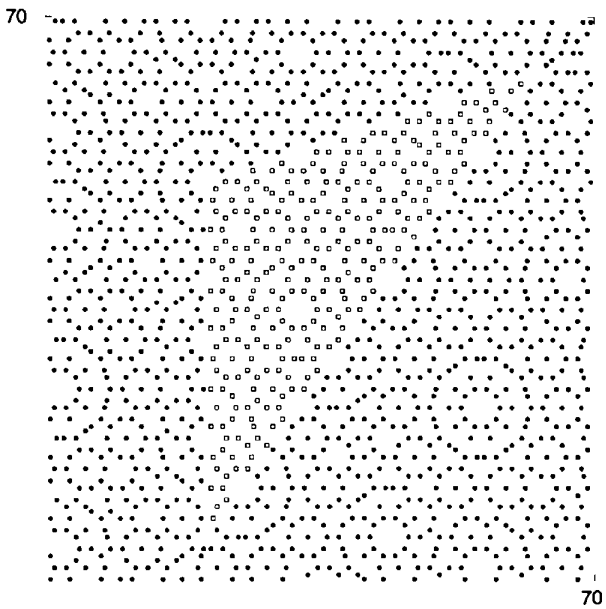

Fig. 7. Projection along **c** ($\mathbf{a}_5$) for a 70 × 70 Å section of the nanodomain structure built from complete monoclinic (4, 6)-approximant unit cells (filled symbols) with atoms from the quasicrystal structure filling domain boundaries (open symbols).

Approximant unit cells are locally selected according to the sum of displacements. The minimum distance for two neighbouring cell centres is restricted to one cell diameter for minimizing overlap. Consequently, domain boundaries are partly left empty. To fill them properly, a growth rule completing the clusters correctly would be needed. For a first crude model, the empty space at the domain boundaries is filled with atoms from the quasicrystalline structure. These regions may represent the remaining original quasicrystal matrix, *i.e.* parts of the structure where the transformation is not yet completed. Since the structural units are identical in both quasicrystal and approximant, the additional

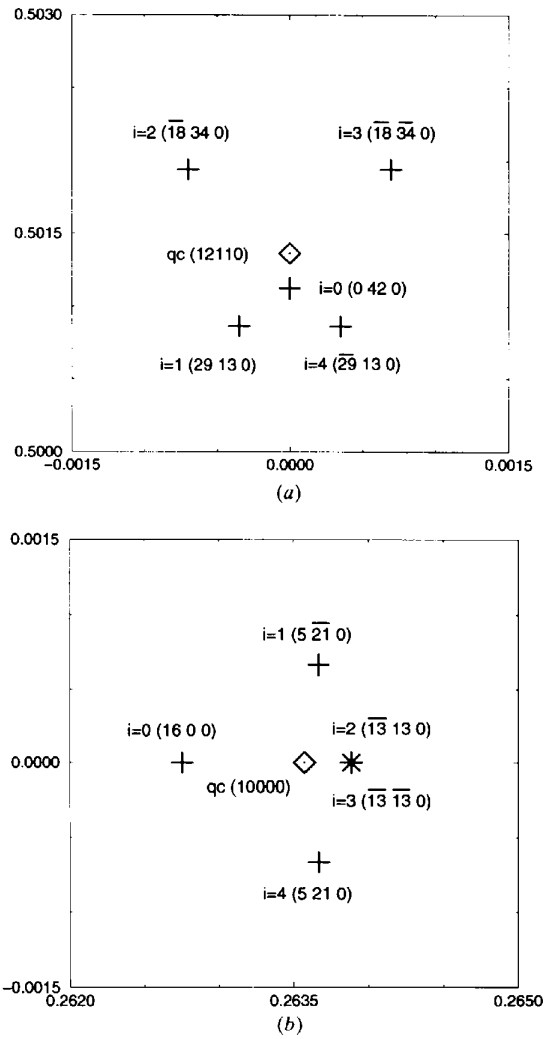

Fig. 8. Calculated Bragg peak positions and indexing for two typical reflection clusters in the vicinity of the quasicrystal peak: 12110 in (*a*) and 10000 in (*b*). The positions for the nanodomain structure are marked by crosses and for the decagonal quasicrystal by diamonds. Labels on the x (h) and y (k) axes are in Å^{-1} referring to the orthorhombic C-centred setting of the nonrotated (4, 6)-approximant. $i = 0, \ldots, 4$ denotes the amount of rotation by $2\pi i/5$ for the approximant orientation the reflections originate from.

atoms fit quite well and complete the structure motifs (Fig. 7).

As expected, simulated diffraction patterns of unfilled and filled domain structures cannot be distinguished as the scattering power of the additional volume is small. Just 2.75% additional atoms are necessary to fill all domain boundaries entirely. The computational effort, however, increases dramatically because an explicit Fourier transform has to be performed for all atoms outside the complete unit cells. However, a significant effect is expected for the distribution and intensity of the diffuse scattering only while the Bragg intensities almost remain invariant.

4.3. *Comparison with HRTEM results*

Most studies on approximants and quasicrystals carried out by transmission electron microscopy (TEM) concentrate on high-resolution (HR) images giving information about the local atomic structure. More global conclusions on the domain arrangement of microcrystalline approximants are scarce. Song *et al.*

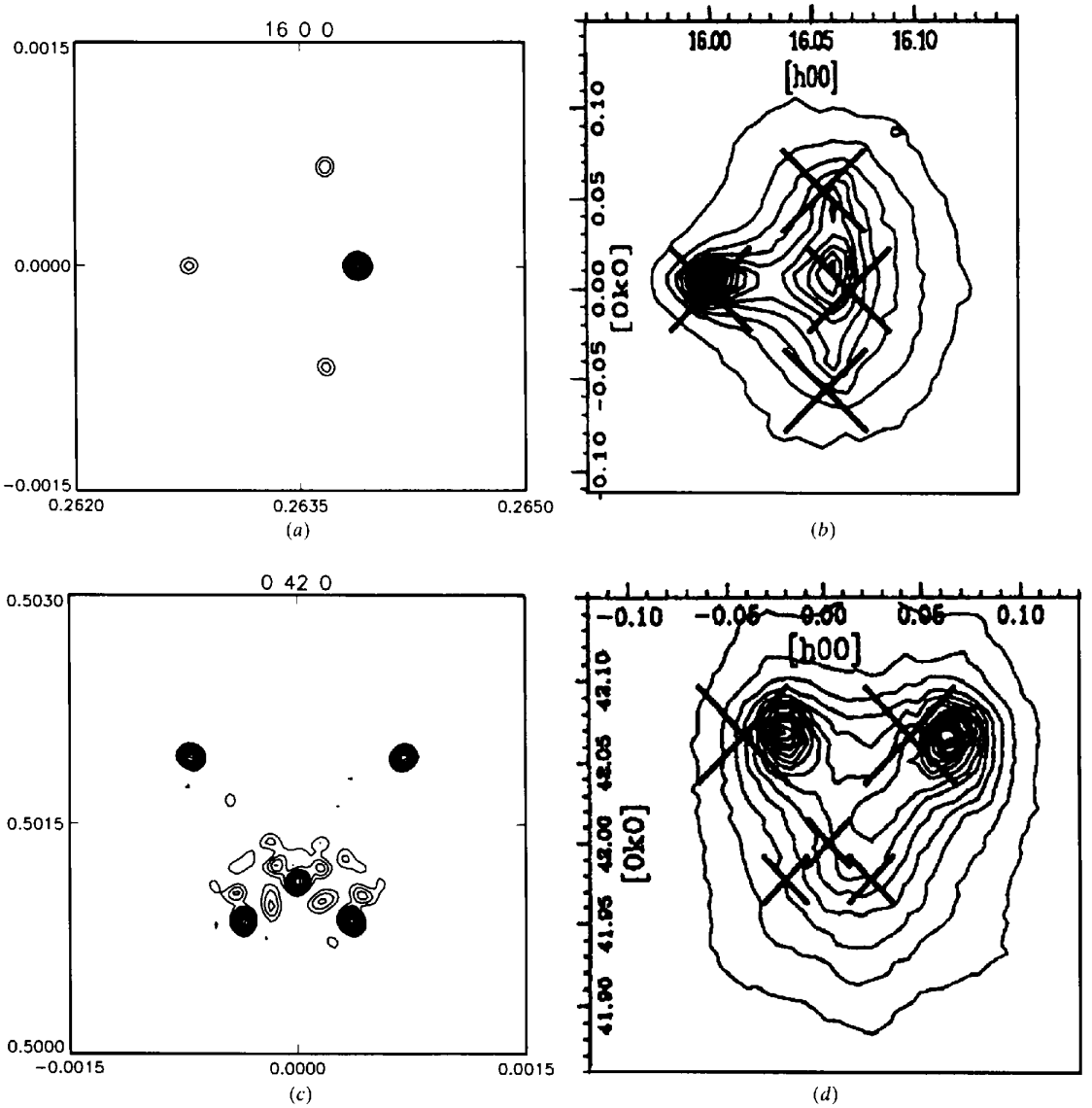

Fig. 9. Comparison of calculated patterns: (*a*), (*c*) for the 8000 × 8000 × 4 Å nanodomain structure model with high-resolution X-ray measurements; (*b*), (*d*) (parts from Figs. 8.5 and 8.6 of Kalning, 1996) at positions of the strongest quasicrystal reflections (*a*), (*b*) 10000 and (*c*), (*d*) 12110. Indices and directions (*h*, *k*) refer to the orthorhombic description of a single nonrotated approximant, dimensions on the simulated plots are in $Å^{-1}$, contour lines are plotted down to 10% of the maximum intensity. Crosses on the experimentally observed patterns indicate the theoretical positions of single approximant reflections in all possible orientations.

(1993) examined nanodomain structures of the (4, 6)-approximant in Al–Co–Cu alloys using TEM to observe lattice fringes. The micrographs show domains with dimensions between 100 Å and more than 1000 Å. Usually, all five possible domain orientations can be observed. There are images with small domains (less than 200 Å) orientated randomly. Furthermore, a nearly star-like arrangement of five differently orientated domain systems, described as jagged bands of widths ranging from 100 to 1000 Å expanding over even larger distances were found (*cf.* Song *et al.*, 1993, Figs. 3*a*, *b*, *d*). These observations closely resemble features present in the nanodomain model resulting from our simulations. However, the average domain size of the simulated structure is comparatively larger.

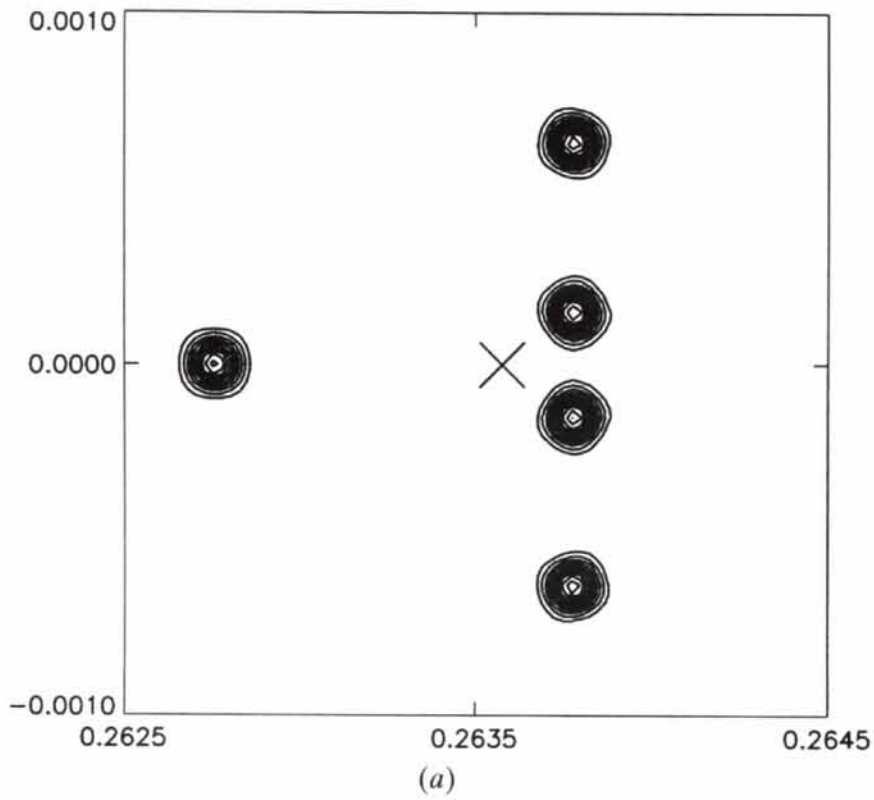

Fig. 10. Comparison of the calculated pattern: (*a*) of an incoherently twinned one-dimensional quasicrystal (8000 × 8000 × 4 Å) with high-resolution X-ray measurements; (*b*) (Fig. 6.7 of Kalning, 1996) at positions around the quasicrystal reflection 10000. Indices and directions (h, k) in the measured pattern refer to the orthorhombic description for a single nonrotated (4, 6)-approximant. Lines indicate the direction of the phason peak shift; the intersecting point is taken as ideal peak position for the decagonal quasicrystal. Dimensions on the simulated plots are in Å^{-1}, the cross gives the exact position of the 10000 reflection for the decagonal structure. Contour lines are plotted down to 10% of the maximum intensity.

5. Reciprocal-space studies

5.1. *Peak positions*

All reciprocal-space vectors **H** of the decagonal quasicrystal are given by equation (5), with respect to an integral indexing and quasicrystal reciprocal-space parameter a_i^* (Steurer & Haibach, 1998*a*). Bragg-peak positions can be represented as vector components on a

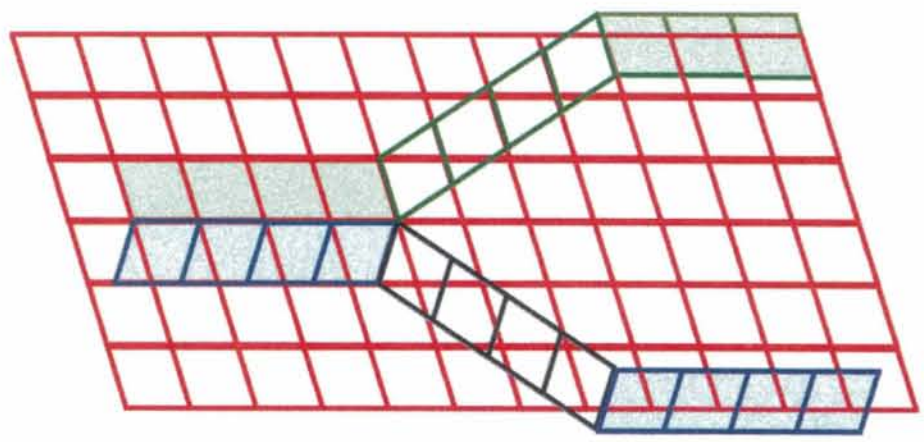

Fig. 11. Schematical representation of the preservation of the phase relationship between equally oriented domains separated by domains of different orientation (*i.e.* being in a reflection-twin relationship). The green-shaded domains preserve their phase relationship along the horizontal direction. The same is true for the blue-shaded domains.

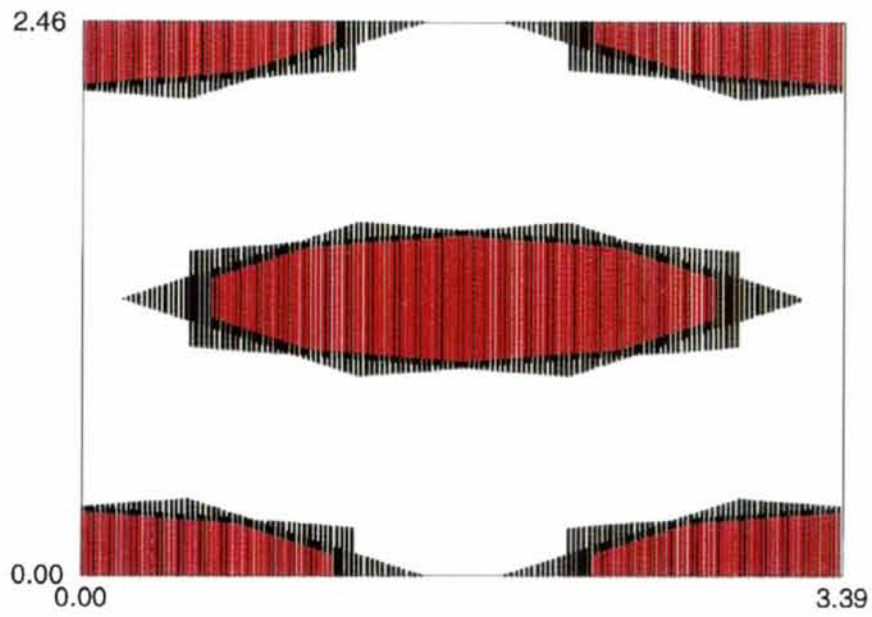

Fig. 12. 1200 × 1200 Å section of the decagonal model structure projected onto one centred orthorhombic unit cell of the average structure. The resulting 'averaged atoms' have the shape of two superposed distorted pentagons (*i.e.* of the atomic surfaces). The unit-cell parameters have been obtained by oblique projection (Steurer & Haibach, 1998*b*). The cell dimensions are given in Å, projected Al atoms are marked by black dots, TM atoms by red dots.

Cartesian coordinate system in physical space:

$$\mathbf{H} = \sum_{i=1}^{5} h_i \mathbf{a}_i^*,$$
$$\mathbf{a}_i^* = a_q^* \big(\cos(2\pi i/5), \sin(2\pi i/5), 0\big),$$
$$i = 1, \ldots, 4 \quad \text{and} \quad \mathbf{a}_5^* = a_5^*(0, 0, 1). \qquad (5)$$

For each orientation of an approximant in the nanodomain structure, Bragg reflections can be indexed with three integers and its positions can be derived as for any periodic structure. In the case of incoherent scattering, peak positions for the complete domain structure result from the simple superposition of the reciprocal lattices of the approximants in five orientations (rotated by $2\pi i/5$, $i = 0, \ldots, 4$). Two reciprocal-space sections are shown in Fig. 8, where in the vicinity of a quasicrystal reflection clusters of approximant Bragg peaks could be observed in high-resolution experiments.

5.2. *Peak widths*

A nanodomain model of $\pm 4000 \times \pm 4000 \times 4$ Å leads to peak widths less than 1.3×10^{-4} Å^{-1} (FWHM). Analogously, an $8000 \times 8000 \times 4$ Å quadrant of the biggest model corresponds to a coherence length of about 8000 Å. For comparison, approximately 2.5×10^{-4} Å^{-1} are found in an ideally fivefold twinned approximant of $\pm 4000 \times \pm 4000 \times 4$ Å, reproducing the 4000 Å maximum extent of a coherently scattering twin individual. Thus, the nanodomain structure with coherent scattering from equally orientated cells, even if separated by domains of another orientation, shows sharper reflections as expected from the domain size. The peak widths are not affected by the size of the individual domains but by the maximum distance between coherently scattering structure motifs. Caused by size and shape of the domains, additional intensities are surrounding strong Bragg peaks (*cf.* Fig. 9*c*).

5.3. *Intensities*

The intensity distribution of the individual split reflections derived from the nanodomain structure indicates strong contributions from coherent scattering. Although the number of approximant unit cells is the same in each of the five possible orientations, peak heights differ by a factor up to three. This can best be seen in the vicinity of the 10000 quasicrystal reflection (Fig. 9*a*), where two approximant peaks coincide perfectly. For example, the summation of the $\bar{1}\bar{3},\bar{1}\bar{3},0$ and $\bar{1}\bar{3},13,0$ reflections belonging to two differently oriented domains (rotated $4\pi/5$ and $6\pi/5$, respectively) leads to a six times larger intensity than the symmetrically equivalent 16,0,0 peak for the not rotated orientation. Thus, differently orientated domains cannot be treated as completely independently scattering. Calculations for differently generated nanodomain structures (see §8) show that the amount of coherent scattering strongly depends on the domain-size distribution.

5.4. *Comparison with experimental results*

Fettweis *et al.* (1994) performed high-resolution X-ray experiments at a synchrotron source (LURE) using the photographic precession technique. Their diffraction pattern analysis by identification of lattice parameters and angles undoubtedly confirms the examined sample to be a microcrystalline twinned (4, 6)-approximant. However, further conclusions concerning unit-cell decoration, domain size and distribution or the nature of domain boundaries were not possible. Recently, a reversible phase transformation between a decagonal quasicrystal and a microdomain structure of this specific approximant was found as a function of temperature (Fettweis *et al.*, 1995).

High-resolution two-dimensional scans in reciprocal space, allowing a comparison with our simulations, are available for several sections of the *hk*0 layer around strong quasicrystal reflections (Kalning, 1996; Kalning *et al.*, 1994). For one of the three samples examined, peak positions are matched best by a twinned (4, 6)-approximant model. The other two specimens are dominated either by the decagonal phase or by a one-dimensional quasicrystal as resulting from linear phason strain (Kalning *et al.*, 1997).

Simulations with five independent sections of a nanodomain model, each $8000 \times 8000 \times 4$ Å, reproduce the diffraction pattern qualitatively very well (Fig. 9). Kalning (1996) observed minimal peak widths of 1.27×10^{-4} Å^{-1} (FWHM) for individual reflections corresponding to a coherence length of 8000 Å. However, the actual peaks in the experimental pattern seem to be broader than the calculated ones. Therefore, regions scattering coherently should be smaller than 8000×8000 Å on average. Calculations for smaller models, on the other hand, are dominated by subsidiary maxima (finite-size effects) allowing no direct comparison. The major deviation between observed and calculated patterns is the intensity distribution of the individual peaks. While the strongest intensity has been observed for the 16,0,0 reflection (Fig. 9*b*), this peak is almost absent in the calculated pattern (Fig. 9*a*). Kalning's experiments as well as the simulations show tenfold symmetry for the intensity distribution, *i.e.* the diffraction patterns are similar around all symmetrically equivalent 10000 quasicrystal reflections. Thus, a strongly unproportional presence of one domain orientation with respect to the five possible can be excluded as a reason for this observation. More likely, the kind of domain distribution and the decoration of the unit cells are responsible for the intensity distribution within the split patterns.

6. One-dimensional quasicrystal as intermediate step in the phase transformation

As mentioned above, various authors propose a one-dimensional quasicrystal to be involved in the phase transformation from a decagonal quasicrystal towards a three-dimensional periodic crystalline approximant (*cf.* Kalning *et al.*, 1997). A structure periodic in two directions and quasiperiodic in the third one can be obtained by a homogeneous deformation (linear phason strain) of the five-dimensional periodic lattice of the decagonal quasicrystal (see §1). The phason strain concept has been worked out for the general decagonal case by Zhang & Kuo (1990). The diffraction vector $\mathbf{H}$ is split into its parallel (physical) and perpendicular space components $\mathbf{H} = \mathbf{H}^{\parallel} + \mathbf{H}^{\perp}$,† omitting the periodic direction $\mathbf{a}_5$ (= $\mathbf{c}$) which is not changed.

$$\mathbf{H}^{\parallel} = \sum_{i=1}^{4} h_i \mathbf{a}_i^{*\parallel}; \quad \mathbf{H}^{\perp} = \sum_{i=1}^{4} h_i \mathbf{a}_i^{*\perp},$$

where

$$\begin{aligned} \mathbf{a}_i^{*\parallel} &= a_q^*[\cos(2\pi i/5)\mathbf{e}_x + \sin(2\pi i/5)\mathbf{e}_y], \quad i = 1, \ldots, 4 \\ \mathbf{a}_i^{*\perp} &= a_q^*[\cos(4\pi i/5)\mathbf{e}_x + \sin(4\pi i/5)\mathbf{e}_y], \quad i = 1, \ldots, 4. \end{aligned} \tag{6}$$

For a one-dimensional quasicrystal resulting from linear phason strain (given as matrix M), the physical space diffraction vector can be formulated as

$$\mathbf{H}^{\parallel}_{1\,\mathrm{dqc}} = \widetilde{\mathbf{H}}^{\parallel}_{2\,\mathrm{dqc}} = \mathbf{H}^{\parallel}_{2\,\mathrm{dqc}} + M\mathbf{H}^{\perp}_{2\,\mathrm{dqc}},$$

where

$$M = \begin{pmatrix} m_{11} & m_{12} \\ m_{21} & m_{22} \end{pmatrix}. \tag{7}$$

Zhang & Kuo (1990) as well as Kalning *et al.* (1997) used the special case where m_{11} is the only non-zero component of M. Then, all Bragg peaks are shifted along the x direction, while the y component remains unchanged with respect to the two-dimensional quasicrystal. It can be shown that the solution for M is unique; leading, together with fivefold twinning, to a diffraction pattern as observed by Kalning *et al.* (1997) (Fig. 10).

Fivefold twinning can be described as a rotation by $-2\pi j/5$ acting on symmetrically equivalent diffraction vectors of domains in orientations rotated by $2\pi j/5$ ($j = 0, \ldots, 4$). In the vicinity of the 10000 quasicrystal reflection, four of the five Bragg peaks in a fivefold twinned one-dimensional quasicrystal form a straight line parallel to $\mathbf{y}$, as the x component of the physical space diffraction vectors results in:

$$h^{\parallel}_{xij} = a_q^*[m_{11}\cos(4\pi i/5)\cos(2\pi j/5) + 1], \quad i = j = 0, \ldots, 4. \tag{8}$$

Combining equation (8) with an alternative equation for the x components of the diffraction vectors deduced using the known h index (in analogy to the nanodomain model) and the formalism for ordinary periodic structures, the 'new' periodicity $a_{1\,\mathrm{dqc}}$, depending on the two-dimensional quasicrystal constant a_q, and the component m_{11} can be derived as

$$\begin{aligned} a_{1\,\mathrm{dpc}} &= 2a_q(\tau^6/5^{1/2}) = 60.893\ldots\ \text{Å}, \\ m_{11} &= 8(5^{1/2}/\tau^6) - 1 = 3.105\ldots \times 10^{-3}. \end{aligned} \tag{9}$$

The simulated diffraction pattern of an incoherently fivefold twinned one-dimensional quasicrystal constructed with this metric fits the observed data quite well (Fig. 10). The periodicity $a_{1\,\mathrm{dqc}}$ is exactly the same as a_o for the C-centred (4, 6)-approximant. Linking the basic clusters is possible with different distances between the cluster centres (as illustrated in Steurer *et al.*, 1993). A long distance L can be assigned using the shortest interatomic vector:

$$L = a_q \tfrac{2}{5}\tau^3(2+\tau)^{1/2} = 19.78\ldots\ \text{Å}. \tag{10}$$

Five clusters in a pentagonal arrangement (superclusters) with edge length L are frequently observed by HRTEM in Al–Co–Ni quasicrystals as well as in approximants (*cf.* Ritsch, 1996). Moreover, two of these superclusters are found to share an edge aligning antiparallel. This structure motif defines exactly the a direction of the centred orthorhombic approximant cell (a_o is perpendicular to the shared edge of the superclusters with a_o as the distance between the outermost cluster centres).

The formation of superclusters in the decagonal quasicrystal along all five possible directions (symmetrically equivalent to the orthorhombic a direction) causes a dentritic growth of a fivefold twinned one-dimensional quasicrystal. For the first several hundred ångströms, shifts are mostly simple flips, while during further propagation other distances appear. This dentritic growth is able to preserve the structure-factor phase relationship over distances larger than the approximant-domain diameters. The phase relation is not lost in one dimension if and only if neighbouring domains have an orientation relationship of $\pm 2\pi/5$ (Fig. 11). Thus, even zigzag chains of adjoining superclusters result in diffraction patterns similar to the twinned one-dimensional quasicrystal and could be a kind of precursor to crystalline nanodomain structures.

7. Scenario for the phase transformation

The results of our simulations on the phase transformation supported by experimental observations indicate the following scenario:

† Illustration and further discussion on reciprocal-space properties in nD space can be found in Steurer & Haibach (1998*a*).

First stage: phason-driven local nucleation of nanocrystalline approximant domains in the quasicrystal matrix by single flips of a small number of atoms. The globally averaged structure of the nanocrystalline domains separated by extended discommensurations is quasiperiodic.

Second stage: quasi-one-dimensional (dentritic) growth of crystalline domains by flips and small atomic displacements. The globally averaged structure corresponds to that of a fivefold twinned one-dimensional quasicrystal.

Third stage: further growth of the approximant domains; energy minimization of the domain structure preserving complete clusters leads to smooth domain boundaries. The resulting average structure is that of a fivefold twinned (4, 6)-approximant with a correlation length far beyond the individual domain size.

8. Influence on the domain distribution of slight structural changes of the periodic approximant

As mentioned in §5.4, the domain distribution resulting from the presented mechanism cannot quantitatively reproduce the observed diffraction patterns (Kalning, 1996) concerning the intensity distribution. To investigate possible reasons, simulations were performed with approximant structures slightly altered in their metrics, as demanded by the following structural considerations.

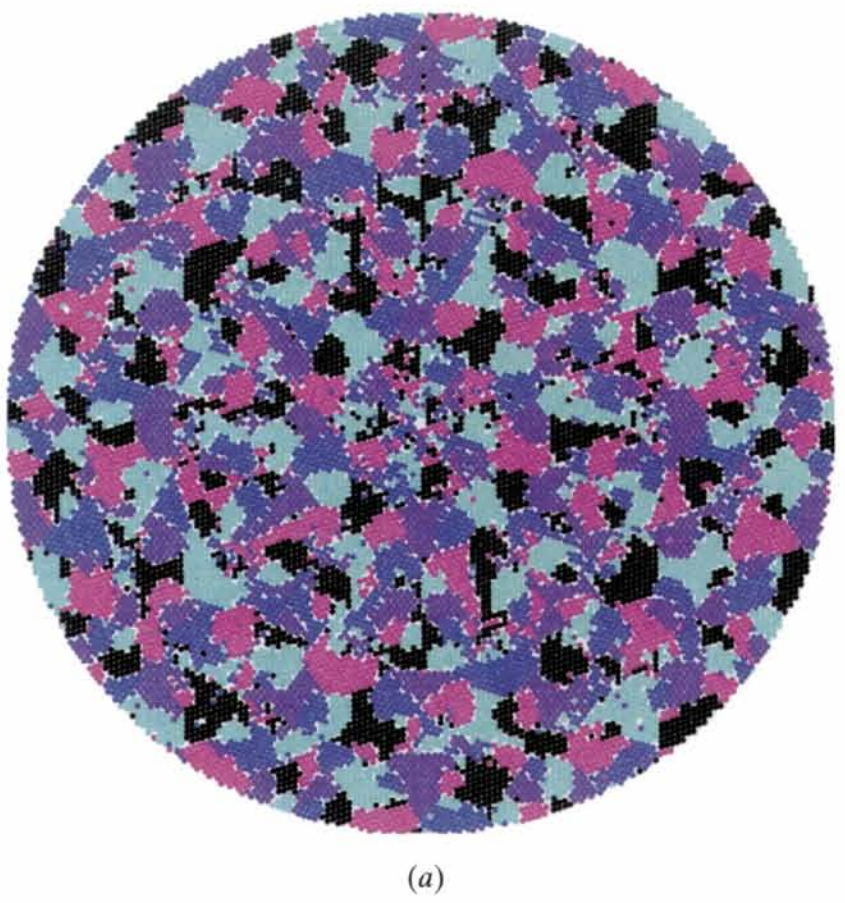

(*a*)

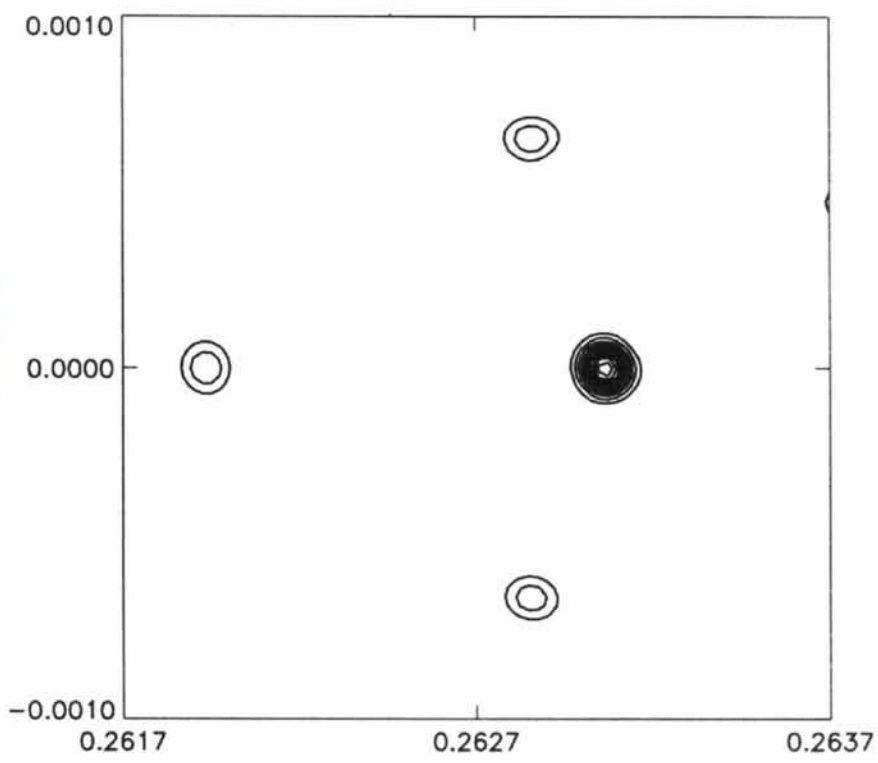

(*b*)

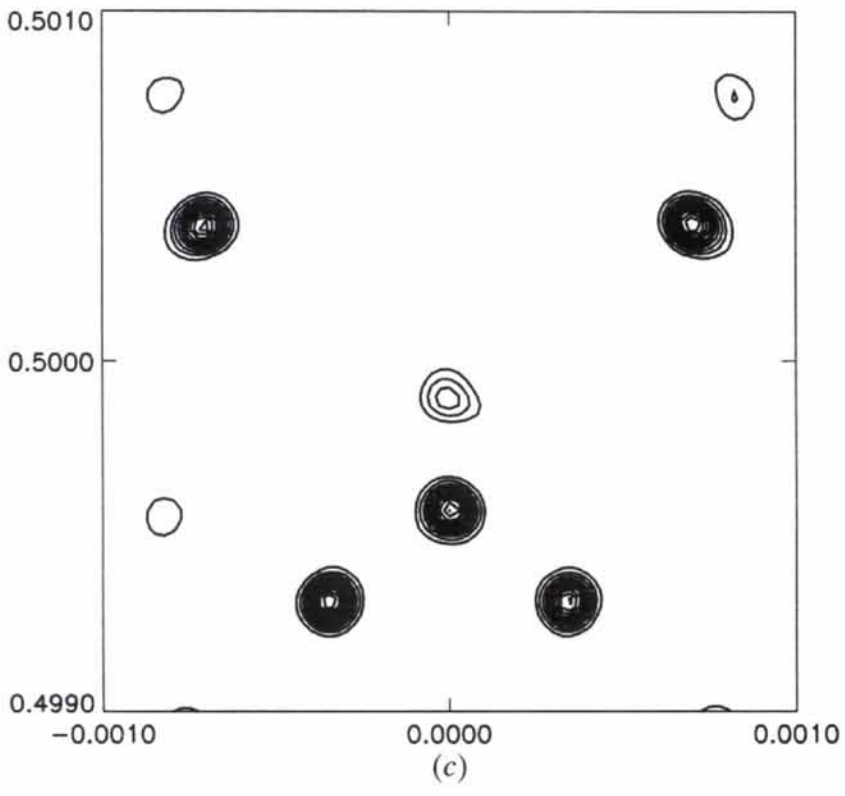

(*c*)

Fig. 13. (*a*) Nanodomain structure resulting from an approximant structure rescaled according to the periodic average structure of the decagonal quasicrystal. The region around the origin is shown (8000 Å in diameter). The different domain orientations are indicated by different colours. The calculated diffraction patterns are shown for the two prominent reflection clusters in the vicinity of (*b*) 10000 and (*c*) 12110 decagonal quasicrystal Bragg peaks based on the nanodomain structure given in (*a*). For (*b*) and (*c*), dimensions are in Å^{-1}, contour lines are plotted down to 10% of the maximum intensity.

8.1. *Effects of the periodic average structure of a decagonal quasicrystal*

Not only one-dimensional quasicrystals like the Fibonacci sequence but also the Penrose tiling has a discrete periodic average structure (Steurer & Haibach, 1998*b*). As the quasicrystal model used here is based on a subset of vertices of a Penrose tiling, it exhibits a two-dimensional average structure as well (Fig. 12). This average structure can be achieved by an appropriate oblique projection of the four-dimensional structure onto the two-dimensional physical space. The metrics of this cell is given by equation (11) for one of the five possible orientations in orthorhombic centred notation, using a_p, the edge length of a Penrose tile and the quasicrystal constant a_q. Note that **a** and **b** vectors were chosen $\mathbf{a} \parallel \mathbf{a}_o$ (approximant) and $\mathbf{b} \parallel \mathbf{b}_o$.

$$a = (3-\tau)a_p a_q; \quad b = (1/\tau)(3-\tau)^{3/2} a_p a_q, \quad \text{with} \quad a_p = \tfrac{2}{5}\tau. \tag{11}$$

Comparing the unit-cell dimensions of the (4, 6)-approximant with those of the averaged quasicrystal structure, one finds a slight mismatch of 3.1‰ in the a direction and less than 0.2‰ in the b direction. Thus, the approximant and the quasicrystal have a common average structure within this mismatch. The presence of a periodic part in the quasicrystal potential and in the mass density waves may be one of the driving forces in the formation of this particular approximant and the domain structure.

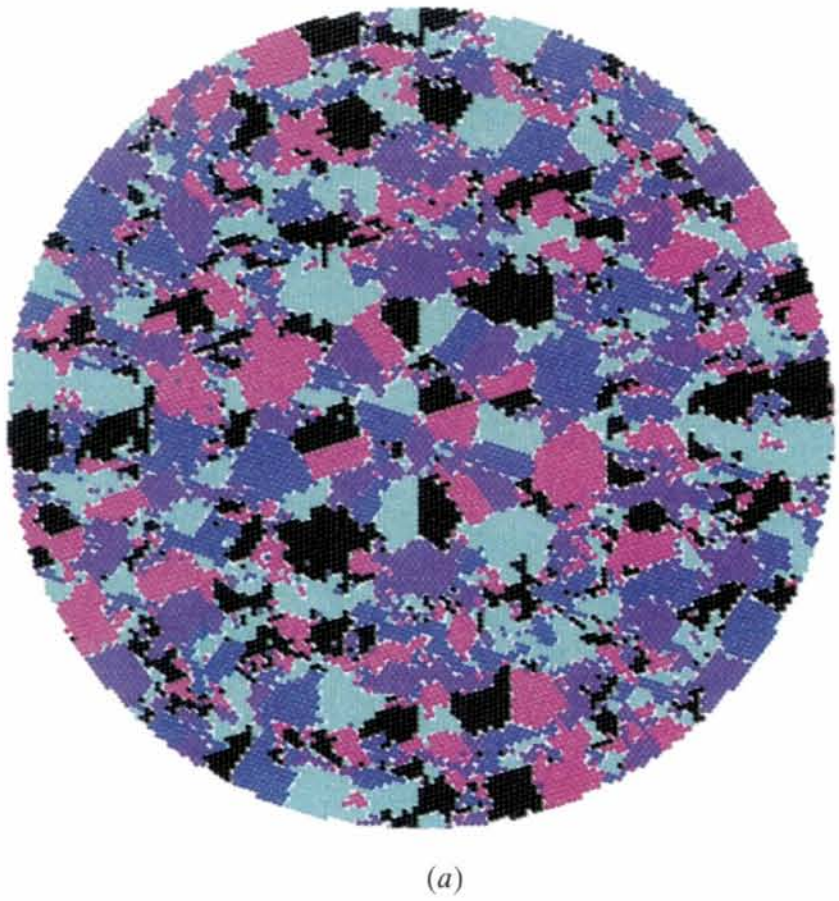

(*a*)

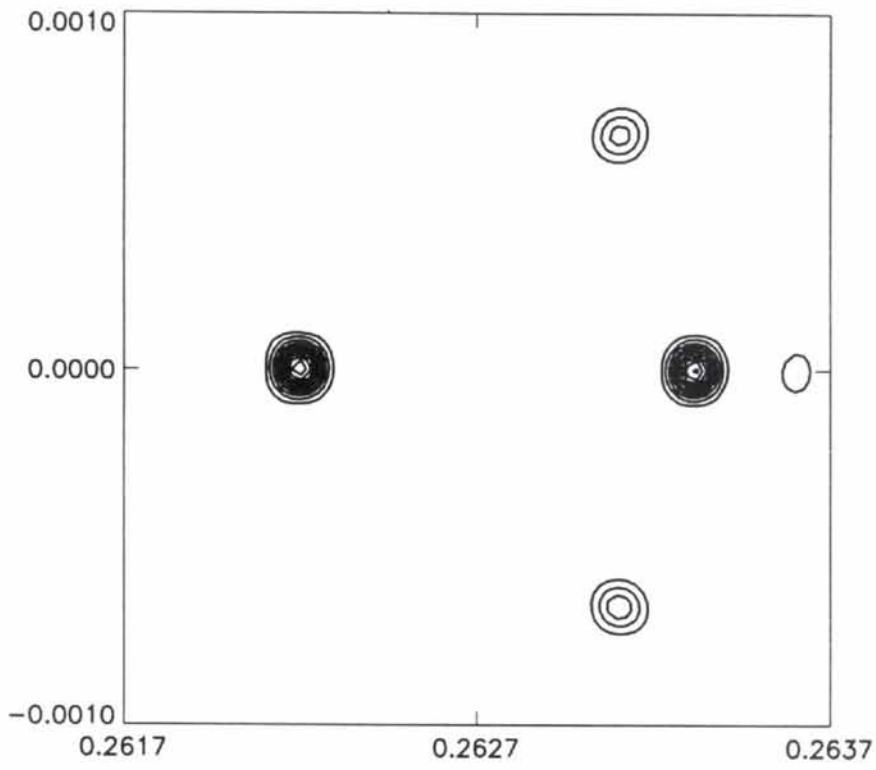

(*b*)

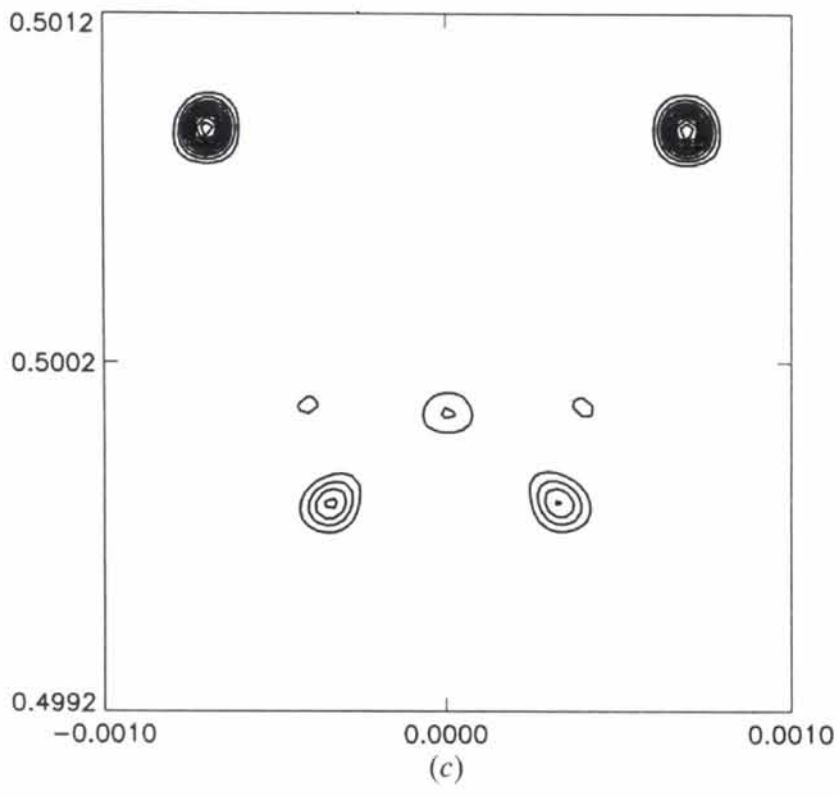

(*c*)

Fig. 14. (*a*) Nanodomain structure around the origin (8000 Å in diameter), resulting from an approximant structure rescaled according to possible layer flattening. The different domain orientations are indicated by different colours. The calculated diffraction patterns are shown for the two prominent reflection clusters in the vicinity of (*b*) 10000 and (*c*) 12110 decagonal quasicrystal Bragg peaks based on the nanodomain structure given in (*a*). For (*b*) and (*c*), dimensions are in Å^{-1}, contour lines are plotted down to 10% of the maximum intensity.

However, scaling all interatomic distances in a way to obtain the approximant being an exact integral superstructure of the averaged quasicrystal unit cell leads to completely different peak arrangements in the diffraction patterns. This can easily be understood from the deviation from the exact 108° angle in the monoclinic unit-cell description. Thus, deformations following the periodic potential have to be homogeneous. Considering the quasi-one-dimensional growth as implication of supercluster ordering, no reason to distinguish between the symmetry-related directions in the decagonal quasicrystal exists. A homogeneous deformation by a factor f scaling a_o to the next integer multiple of a ($f = 18/\tau^6$) was applied. Subsequent calculations as described in detail above lead to a nanodomain structure with many very small individual approximant domains (mostly less than ten unit cells in diameter) that still mimic the quasicrystal symmetry with a kind of noisy distribution in the central part (Fig. 13*a*). The 16 400 unit cells are equally distributed between the five possible orientations (for each 3280 cells are present). Fourier transformation of this single $8000 \times 8000 \times 4$ Å model shows surprisingly less subsidiary maxima. Nevertheless, it is nearly identical to the patterns observed from the original nanodomain structure, apart from an overall metric scaling (Figs. 13*b*, *c*).

As the actual change in atomic positions is very small, the volume does not increase remarkably during the phase transformation of the decagonal quasicrystal to the rescaled approximant. Consequently, no strong strain fields in the partly transformed sample are to be expected. It is noteworthy that the scaling applied here can easily be included into the deformation of the nD periodic lattice necessary to derive an approximant for the decagonal quasicrystal.

8.2. *Flattening of puckered atomic layers in the quasicrystal*

The idealized quasicrystal structure consists of two flat layers *Aa* (§2.1). However, the structure this model is based on should show a puckering of about ±0.3 Å in one of the layers (Steurer *et al.*, 1993). This puckering plays a certain role in ordering transformations in decagonal Al–Co–Ni quasicrystals (Steurer *et al.*, 1998). For a puckering of ±0.3 Å, a slight flattening by ~0.05 Å would result in a 2‰ expansion of the clusters in the (xy) plane. Unfortunately, no reliable information concerning puckering is available.

Model calculations have been performed with the lattice constant of the monoclinic approximant expanded by 2‰ to 51.90 Å. The calculations give a different domain distribution (Fig. 14*a*). The individual domains are still rather small but on average larger than for the domain model described in §8.1. Especially in the central part, the domains are shaped regularly with straight lines defining the domain boundaries. In the outer parts, larger and smaller domains appear in alternating rings. In total, 16 417 cells are present, about 3300 in each possible orientation. Simulated diffraction patterns for this nanodomain structure ($8000 \times 8000 \times 4$ Å) qualitatively show the same typical reflection clustering as the preceding models. In contrast, they reproduce the intensity distribution within the pattern as was observed experimentally by Kalning (1996) quite well (compare Figs. 14*b* and *c* with 9*b* and *d*).

9. Concluding remarks

A mechanism is presented for the transformation from the decagonal Al–Co–Ni phase to an orientationally twinned crystalline nanodomain structure *via* an intermediate one-dimensional quasiperiodic state, based on only small atomic displacements. It leads to small domains with correlation length far beyond the individual domain size. The simulations are in good agreement with the experimental observations in direct (HRTEM studies) as well as in reciprocal space (high-resolution X-ray diffraction).

For an experimental proof of the suggested mechanism, very accurate high-resolution X-ray diffraction studies are needed. Quasicrystal and approximant lattice parameters have to be measured as a function of temperature on one and the same sample during the reversible phase transformation.

We would like to acknowledge financial support by Swiss National Science Foundation contracts 21-40249.94 and 20-46717.96.

References

Audier, M., Guyot, P., de Boissieu, M. & Menguy, N. (1993). *J. Non-Cryst. Solids*, **153&154**, 591–594.
Baumgarte, A., Schreuer, J., Estermann, M. A. & Steurer, W. (1997). *Philos. Mag.* A**75**, 1665–1675.
Coddens, G. & Launois, P. (1991). *J. Phys. I (Paris)*, **1**, 993–998.
Dong, C., Dubois, J. M., de Boisseu, M. & Janot, C. (1991). *J. Phys. Condens. Matter*, **3**, 1665–1673.
Duneau, M. & Oguey, C. (1990). *J. Phys. (Paris)*, **51**, 5–19.
Edagawa, K., Suzuki, K., Ichihara, M. & Takeuchi, S. (1991). *Philos. Mag.* B**64**, 629–638.
Estermann, M. A., Haibach, T. & Steurer, W. (1994). *Philos. Mag. Lett.* **70**, 379–384.
Fettweis, M., Launois, P., Dénoyer, F., Reich, R. & Lambert, M. (1994). *Phys. Rev. B*, **49**, 15573–15587.
Fettweis, M., Launois, P., Reich, R., Wittmann, R. & Dénoyer, F. (1995). *Phys. Rev. B*, **51**, 6700–6703.
Goldman, A. I. & Kelton, K. F. (1993). *Rev. Mod. Phys.* **65**, 213–230.
Hiraga, K., Sun, W. & Lincoln, F. J. (1991). *Jpn. J. Appl. Phys.* **30**, L302–L305.
Janssen, T. (1991). *Europhys. Lett.* **14**, 131–136.

Kalning, M. (1996). PhD thesis, Christian-Albrechts-Universität zu Kiel, Germany.
Kalning, M., Kek, S., Burandt, B., Press, W. & Steurer, W. (1994). *J. Phys. Condens. Matter*, **6**, 6177–6187.
Kalning, M., Kek, S., Krane, H. G., Dorna, V., Press, W. & Steurer, W. (1997). *Phys. Rev. B*, **55**, 187–192.
Qin, Y., Wang, R., Wang, Q., Zhang, Y. & Pan, C. (1995). *Philos. Mag. Lett.* **71**, 83–90.
Ritsch, S. L. (1996). PhD thesis, Swiss Federal Institute of Technology Zürich, Switzerland.
Song, S., Wang, L. & Ryba, E. R. (1993). *J. Mater. Sci. Lett.* **12**, 80–83.
Steurer, W. & Haibach, T. (1998*a*). *International Tables for Crystallography*, Vol. B, edited by U. Shmueli, Section 4.6. In the press.
Steurer, W. & Haibach, T. (1998*b*). In preparation.
Steurer, W., Haibach, T., Zhang, B., Kek, S. & Lück, R. (1993). *Acta Cryst.* B**49**, 661–675.
Steurer, W., Honal, M. & Haibach, T. (1998). *Proceedings of 6th International Conference on Quasicrystals ICQ6*. Singapore: World Scientific. In the press.
Tolédano, P. & Dmitriev, V. (1996). *Reconstructive Phase Transitions in Crystals and Quasicrystals*. Singapore: World Scientific.
Yacamán, M. J. & Torres, M. (1993). Editors. *Crystal–Quasicrystal Transformations*. Amsterdam: Elsevier.
Yamamoto, A. (1996). *Acta Cryst.* A**52**, 509–560.
Zhang, H. & Kuo, K. H. (1990). *Phys. Rev. B*, **41**, 3482–3487.
Zhang, H., Li, X. Z. & Kuo, K. H. (1993). *Crystal–Quasicrystal Transitions*, edited by M. J. Yacamán & M. Torres, pp. 1–12. Amsterdam: Elsevier.
Zhang, H. & Urban, K. (1992). *Philos. Mag. Lett.* **66**, 209–215.